40th European Rotorcraft Forum
Southampton, 2-5 September, 2014
Paper 31

CFD ANALYSIS OF PROPELLER NOISE

C. S. JOHNSON AND G.N. BARAKOS

CFD Laboratory, School of Engineering
University of Liverpool, L69 3GH, U.K.
http://www.liv.ac.uk/cfd
C.S.Johnson@liverpool.ac.uk, g.barakos@liverpool.ac.uk

Abstract

This paper presents CFD results for flows around propellers and compares their aerodynamics performance as well as their aero-acoustics. After some validation of the employed CFD method using wind tunnel experiments, a modern propeller design was assessed. Using the same baseline blade, different propellers were put together by adding stagger at the blade hub and small variations of the inter-blade angle. The employed method produced results showing differences in the propeller acoustics regarding the frequency spectrum produced by each design and the level of the acoustic tones. Installed and un-installed blades were also compared and the results show that the wing, nacelle and fuselage of the blades influence the obtained level of noise but not the frequency content. Computations for a climbing case also show the strong effect of the flight conditions on the acoustic results.

1 INTRODUCTION

Research in propeller acoustics is fuelled by the need for transport aircraft with low impact on airport and community noise and high propulsive efficiency. Previous work on propeller aerodynamics and acoustics includes the work by Jeracki and Mitchell [3] where the SR propeller series was used to test advanced design concepts for high speed turboprop aircrafts. Different number of blades, planform designs and conditions were tested and compared. Acoustic research is also presented by Woodward and Loeffler [10] and McCurdy [5]. Interior fuselage noise was measured on a SAAB 2000 aircraft and reported by Samuelsson et al. in [4]. Differences in starboard and port noise were found and interference from other aircraft components were analysed.
In this paper Computational Fluid Dynamics is used as a tool for comparing the acoustics of different propeller designs revealing differences in noise as a result of modifying the arrangement of the blades on the rotor hub. The effect of having a propeller installed on an aircraft is also investigated and contrasted with results for isolated propeller acoustics. This work is part of the IMPACTA project of GE-DOWTY that provided the baseline blade design. Starting from a given blade shape, different hub arrangements are compared with CFD in terms of their acoustics.

2 GEOMETRY AND CONDITIONS

The IMPACTA propeller is designed for high efficiency at high speeds due to its swept back blades, large number of blades and thinner sections. Its larger diameter allows for less power loading even though more thrust is obtained. This improves the efficiency as it reduces the amount of swirl in the wake due to engine torque. The design is an 8-bladed propeller of aspect ratio 10.4 and root chord length of 0.213 metres. It is modified by introducing staggering of the blades near the hub or by changing the inter-blade angles in a symmetric way. Moving four out of the eight blades slightly forward is expected to change the acoustic signature of the blades and provide a different distribution of the emitted acoustic energy between frequencies. The same effect is expected by changing the inter-blade angle between every other blade of the propeller. The blades are designed to run at an RPM of 856. Figure 1 presents the different hub arrangements. In addition, an offloaded tip variation of the baseline blade was also analysed. The offloaded blade has about 1.8^o less twist than the baseline blade and approximately 2 degrees more pitch at 0.7R/c. It is also run at a different RPM of 790. Figure 2(a) shows the difference.

2.1 Conditions for Computations

Several flight conditions were selected and the ones used for comparisons are summarised in Table 1. The rotation speed is Ω = 89.7 rad/s. The coefficient of thrust is given by the following equation:

$$C_T = \frac{T}{\rho\omega^2 D^4} \tag{1}$$

where D is the diameter of the propeller. The conditions at altitude can be found using:

$$P = P_o\left(1 - \frac{Lh}{T_o}\right)^{g/RL}, \tag{2}$$

$$\rho = \frac{P}{RT}, \tag{3}$$

$$T = T_o - Lh. \tag{4}$$

where P is the Pressure at altitude, P_o is the atmospheric pressure at sea level, L is the temperature lapse rate, h is the altitude, T_o is sea level standard temperature, T is the temperature at altitude, g is the gravitational acceleration, R is the molar mass of air, and ρ is its density at altitude.

The Reynolds number was found to be approximately 1 million based on the root chord of the blade. The speed of sound at this altitude is given by

$$a_o = \sqrt{\gamma RT}, \tag{5}$$

and therefore the tip Mach number was 0.627.

3 CFD METHOD

CFD is used as the primary tool for analysing the acoustics of the propellers. The Helicopter Multi-Block Method (HMB2) is used, taking advantage of its ability to perform steady-state periodic or fully unsteady computations [2] using the RANS and URANS approach or even SAS [6] and DES [8]. For this work, fine multi-block grids were used with the sliding plane method [9] to account for the relative motion between the airframe and the propeller. Propeller grid sizes were approximately 12 million cells per blade for the isolated cases. It is assumed that the propeller blades are rigid. The grid size for the installed cases was about 50 million.

For the cases presented up to date, the Reynolds Averaged Navier-Stokes (RANS) method was used with the $\kappa - \omega$ turbulence model to obtain some preliminary results quickly with the aim of developing a method to analyse the acoustic data. HMB solves the RANS equations in integral form and discretises using a cell-centred finite volume approach on structured multi-block grids. Temporal integration is done using an implicit dual-time stepping method. The details of the theory behind this method and the derivation of its equations can be found in Anderson [1].

The acoustic analysis is carried out using the sound pressure level (SPL) at specified probe locations. These SPLs are obtained using the unsteady pressure obtained from the CFD solution. The primary objective of the acoustic analysis is to determine the noise heard by passengers on an aircraft. Therefore, the time and space resolution required must be such that the frequencies detected are within the audible range (20 - 10000 Hz). Using Nyquist's theorem, to capture 10 kHz, means that the sampling frequency required is 20 kHz. Therefore the largest time step required is 5×10^{-5} seconds. Since the rpm of the propeller is 856 rpm, this means that an azimuth of 1 degree takes approximately 1.94×10^{-4} seconds. Therefore a time resolution of about a quarter degree is required to capture the audible frequencies.

For the spacial or grid resolution, a frequency of up to 4000 Hz should be able to be resolved directly as tonal noises. Higher frequencies are expected to be due to broadband noise. If a frequency of 4000 Hz at the cruise conditions is to be obtained, the wavelength to be resolved can be found as:

$$\lambda = v/f = 0.08m \tag{6}$$

Using a velocity of 316 m/s, since this is the speed of sound at the selected conditions, if 10 points are used to describe the shape of the wave, then a grid resolution of 0.008 metres is required. Therefore the non-dimensional resolution of the grid can be calculated using the reference length, which in this case is the root chord of the blade as 0.0371 c. The nearest probe on the fuselage was 1 metre away from the blade. Therefore, at least 126 cells were needed between the blade and the fuselage. In the mesh used for the computations, there are 112 cells distributed such that the boundary later is captured.

4 CFD VALIDATION USING THE JORP PROPELLER

The JORP model blade was used for comparisons with experiments. It consisted of a single row of six blades mounted on a minimum interference spinner. The blade sections used were high speed designs from the ARA-D/A family and were incorporated at 0.6 and 0.95 r/R. A parallel nacelle was included at 0 pitch and yaw. The diameter was 0.914m (3ft) to create a higher disc loading. 28 pressure tappings were incorporated at each of the 9 radial stations between 0.35 and 0.95 r/R [7]. Typical cruise speeds were at Mach 0.65 for the un-swept blade. The tip speed was 180m/s. Figure 3 shows the geometry of the un-swept version of the JORP. Since the propeller is 6-bladed and the simulation can be assumed to be periodic, only one blade was simulated with periodic boundary conditions on the planes between blades. For one blade, the mesh contained approximately 12 million cells. The distribution is shown in Figure 3. The far-field was placed approximately 5 propeller radii away from the blade [9]. The hub was modelled as a cylinder for faster convergence of the steady-state simulation.

Figure 4 shows the C_p distribution in comparison to the experimental data at a number of radial locations along the blade. The C_p is obtained from the surface pressure distribution. The results agree even if no attempt was made to pitch the blade to optimise the thrust.

5 CFD RESULTS FOR THE IMPACTA BLADE

The topology used for the propeller grids is the same as that of the JORP mesh. The isolated blades each have about 12 million cells. Figure 5(a) shows the propeller installed on the aircraft on the port side. For the installed cases the block and mesh data for each component is given in Table 2. Each of these components was separated by a sliding plane. Some of these sliding planes are shown in Figure 5(b).

5.1 Isolated Propeller Aerodynamics

Figure 6 shows C_p at stations along the radius of the isolated baseline blade with the Baseline, Staggered and Unequal hubs. There is not much change on the blade loading due to the changes in the hub. Figure 7 compares the C_p of the two

different blades i.e. the baseline, and offloaded designs with the baseline hub. The offloaded is pitched higher and hence has more loading inboards. The method used was periodic steady RANS simulations. Unfortunately experimental data is not yet available to validate the CFD results. Figure 8 shows the normal and axial force distributions along the blades.

5.2 Isolated Propeller Acoustics

Figure 9 shows the probe positions where acoustic data is extracted from the CFD solution. The probes are on a fuselage that is at least 1 metre away from the tip of the blade. In this case, the results shown are for the propeller on the port side of the aircraft. Probe 776 is in the middle of the fuselage and inline with the blade hub. Probes 760 and 792 are on the same line but on top and below the fuselage. Although computations were performed in isolation without any nacelle or fuselage, the CFD was able to show the differences between the designs. An example of the spectrum is shown in Figure 10. The peaks from such a curve at the blade passing frequency are plotted in Figure 11 which shows the sound pressure levels (SPL) spectrum for each of these probes with the different variations of hubs and blades. The figures show the maximum amplitude at the blade passing frequencies. It is clear that for the staggered and unequally spaced blades, additional peaks occur at the 4 per rev blade passing frequencies. This is because for these cases, there is a 4-per-rev periodicity either due to blade axial or azimuthal position. Even though, having these additional peaks increases the overall energy of the sound, the additional frequencies makes the periodicity of the signal less detectable and this changes the quality of the noise. In all three probes in line with the propeller plane, the baseline noise diminishes relatively quickly at higher frequencies. The offloaded tip generally has a slightly lower noise profile as well as a different BPF due to its lower rpm conditions. The approximate pitch angle at the 70% radial station in degrees is 50.1 for the Baseline, and 53.6 for the Offloaded blade.

A comparison is also made between unsteady and steady simulations as well as between two unsteady methods: URANS and the Scale Adaptive Simulation (SAS) developed by Menter [6]. Figure 12 shows this comparison for probe 776. Here, the unsteady pressure was estimated by removing the rms pressure over one period. It can be seen that the tonal noise has about the same amplitude but the broadband noise is higher with the unsteady calculations.

5.3 Installed Propellers

Further results were obtained for installed configurations of the propellers using a half-model of a generic turbo-prop aircraft and the same blades and hubs. An example of the surface C_p on the wing, nacelle, and fuselage is shown in Figure 13. The comparison shows the differences between cruise and climb flight conditions. Figure 15 compares the C_p plot of the isolated and installed baseline. The installed blade is at 0 degrees azimuth i.e. vertically upwards. It has a significant drop in load due to the added aircraft components and this impacts on the noise produced. Figure 14 shows the effect of the propellers on the wing loading of the aircraft, in particular, the lift distribution. It is given as a ratio of the loading to the baseline loading, hence a value of one for the baseline case itself. All the solutions are at presented for the same blade azimuth. For the staggered blade, the differences in loading may be due to the fact that it also has a smaller hub and one set of the blades is closer to the wing. The offloaded blade is pitched higher, but its pitch distribution changes a lot between the root and tip of the blade. This may be the cause of the difference in the variation of the load. Figure 16 shows the locations of all the probes for the installed cases. Figure 17 shows the frequency spectrum at one of these probes, probe 776 which is in the same plane as the propeller. It compares the spectrum for the installed and isolated propeller. There is quite a big difference in the broadband noise. However, the key comparison is in the peaks of the harmonics. In this case, the installed case has a louder SPL at the 1st blade passing frequency (BPF) and then drops off faster than the isolated.

6 CONCLUSION

The paper presents the differences in the tonal acoustics of the assessed propeller designs and discusses the benefits of the different hub arrangements in terms of the acoustic tones and their magnitude. It also shows some of the differences between isolated and installed propeller noise simulations. Further work is to be carried out with the installed cases, as well as comparisons with experiments. The isolated blade calculations predicted a change in the frequency content due to modifications of the hub. On the other hand, the level of the tones was not substantially reduced.
The installed case showed an increase in the first harmonic and slightly further drops at the higher frequencies. The results indicated differences due to the presence of the wing, and suggest that comparisons between installed blades are required.

Acknowledgement This work is part of the IMPACTA project of GE-DOWTY and TSB with the University of Liverpool, Aircraft Research Association Ltd, and NLR of The Netherlands as partners.

REFERENCES

[1] John D Anderson, Jr. *Computational Fluid Dynamics, The Basics with Applications*. McGraw-Hill International Editions, 1995.

[2] A. Brocklehurst, R. Steijl, and G.N. Barakos. CFD for tail rotor design and evaluation. In *34th European Rotorcraft Forum*, Liverpool, UK, September 2008.

[3] R.J. Jeracki and G.A. Mitchell. Low and high speed propellers for general aviation - performance potential and recent wind tunnel test results. *NASA Techincal Memorandum*, 81745, April 1981.

[4] S. Leth, F. Samuelsson, and S. Meijer. Propeller noise generation and its reduction on the saab 2000 high-speed turboprop. *AIAA Journal*, 98(2283), 1998.

[5] D.A. McCurdy. Annoyance caused by advanced turboprop aircraft flyover noise. *NASA Techincal Memorandum*, 2782, March 1988.

[6] F. R. Menter and Y. Egorov. Sas turbulence modelling of technical flows. *Direct and Large-Eddy Simulation VI*, 10:687–694, 2006.

[7] N. Scrase and M. Maina. The evaluation of propeller aeroacoustic design methods by means of scaled-model testing employing pressure tapped blades and spinner. In *Proceedings of the 19th ICAS Congress*, Anheim, CA, USA, 18-23 September 1994.

[8] P.R. Spalart, W-H. Jou, M. Strelets, and S.R. Allmaras. Comments on the Feasibility of LES for Wings, and on a Hybrid RANS/LES Approach. In *Proceedings of the 1st AFOSR International Conference On DNS/LES, Columbus, OH, August 4–8,*, 1997.

[9] R. Steijl, G.N. Barakos, and K. Badcock. A framework for CFD analysis of helicopter rotors in hover and forward flight. *International Journal for Numerical Methods in Fluids*, 51:819 – 847, 2006.

[10] R.P. Woodward and I.J. Loeffler. In-flight source noise of an advanced large-scale single-rotation propeller. *Journal of Aircraft*, 30(6), Nov-Dec 1993.

	CRUISE	CLIMB
Altitude (m)	7620	6096
Temperature (ISA + ^{o}C)	10	10
Cruise Mach Number	0.5	0.44
Required thrust (N)	7851.11	12721.91
Tip speed (m/s)	198.12	198.12
RPM	856.14	856.14
Pressure at altitude (Pa)	37581	46544
Density at altitude (kg/m^3)	0.527	0.627
Temperature at altitude (K)	248.6	258.5
Speed of sound (m/s)	316	322

Table 1: *Cruise and climb flight conditions employed for computation.*

Grid Component	No. of Blocks	No. of Cells
Fuselage	208	4,566,404
Nacelle	1556	11,399,377
Wing	118	2,368,258
Baseline Propeller	3664	22,515,696
Staggered Propeller	2704	31,224,832
Unequal Propeller	2704	31,224,832

Table 2: *CFD grid components and their sizes.*

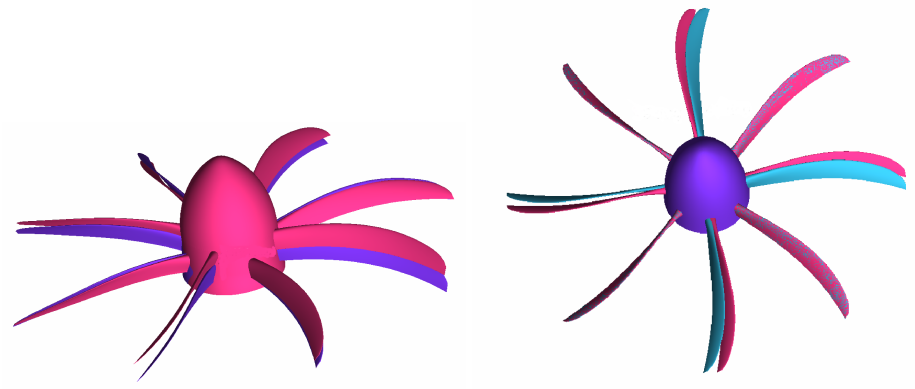

(a) (b)

Figure 1: Comparison of (a) Baseline and Staggered, and (b) Baseline and Unequally-spaced cases.

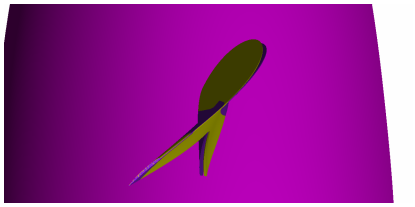

(a)

Figure 2: Comparison of Baseline and Offloaded blades.

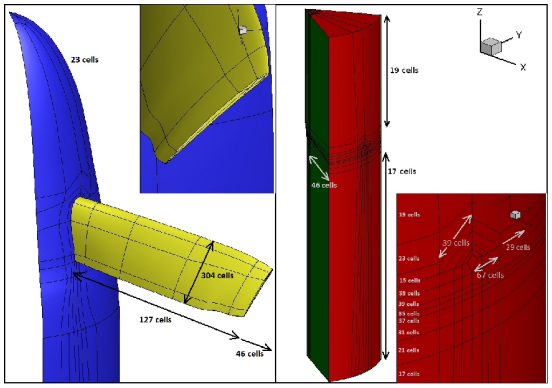

Figure 3: Grid geometry for the un-swept version of the JORP blade. The blue region is the spinner. The red colour represents the far field boundaries.

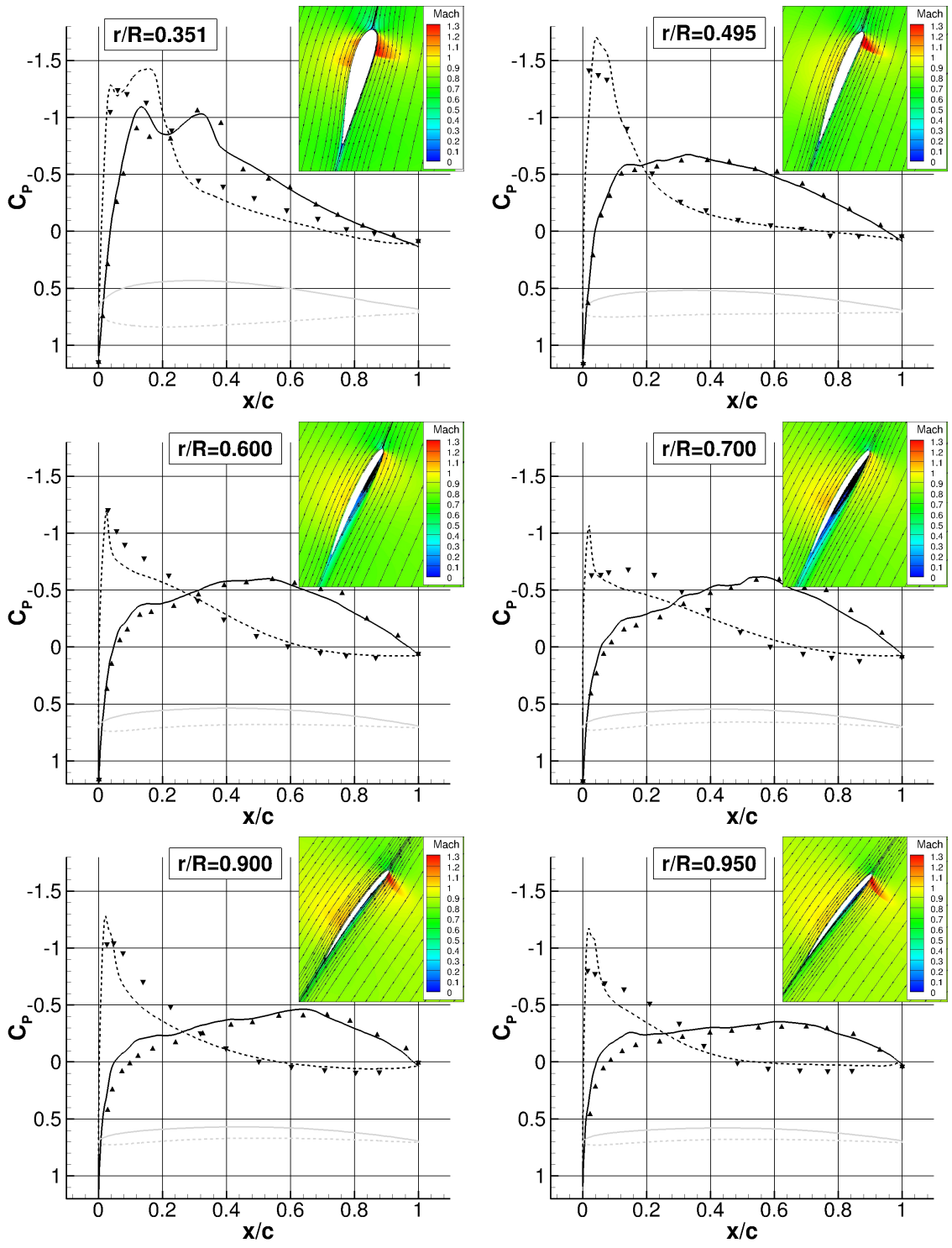

Figure 4: C_p distribution at a number of sections along the blade where experimental comparison can be made. The Mach number field is shown in the insert.

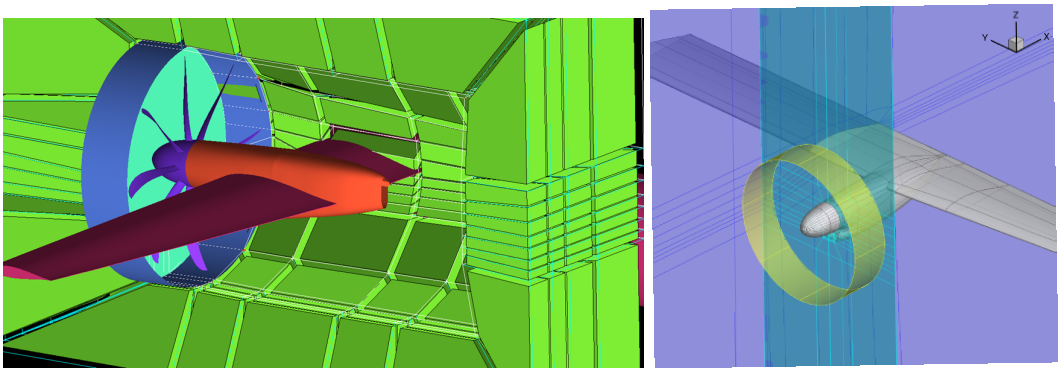

(a) (b)

Figure 5: Multi-block topology and the sliding planes between the propeller and wing.

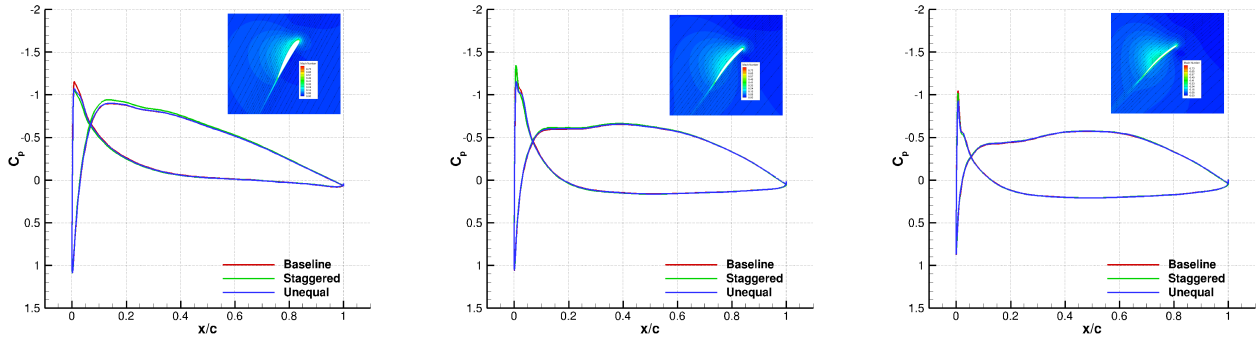

(a) (b) (c)

Figure 6: C_p for the Baseline, Staggered and Unequal hub with the baseline blade at three sections: (a) r/R = 0.5, (b) r/R = 0.7 and (c) r/R = 0.9. Cruise conditions, free-stream Mach = 0.5, tip Mach = 0.627, RANS calculations.

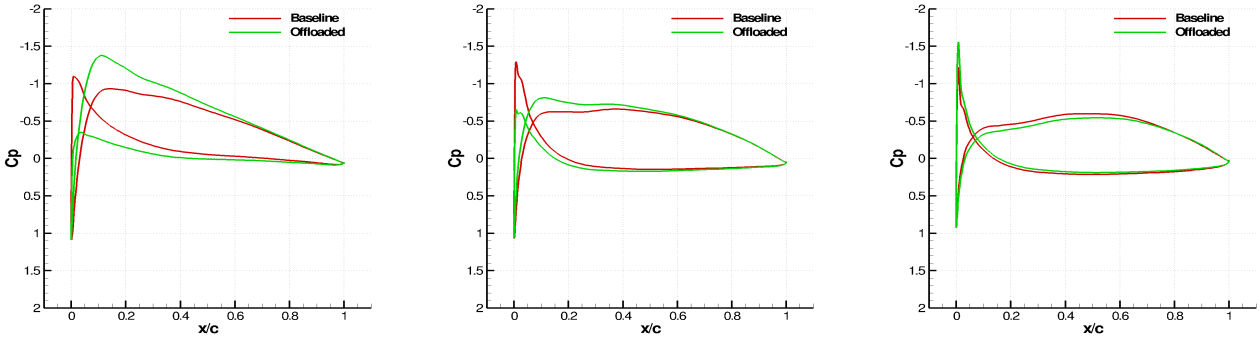

(a) (b) (c)

Figure 7: C_p comparisons for the baseline, and offloaded blades at three sections: (a) r/R = 0.5, (b) r/R = 0.7 and (c) r/R = 0.9. Cruise conditions are given in Table1. For the offloaded blade the tip Mach number was 0.579.

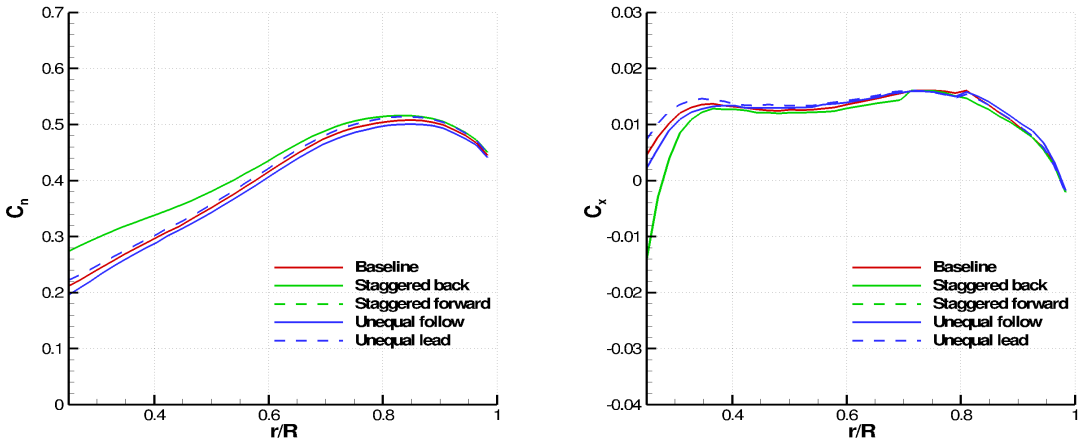

(a) (b)

Figure 8: Normal and axial force distribution for the isolated blades at cruise conditions, free-stream Mach = 0.5, tip Mach = 0.627, RANS calculations.

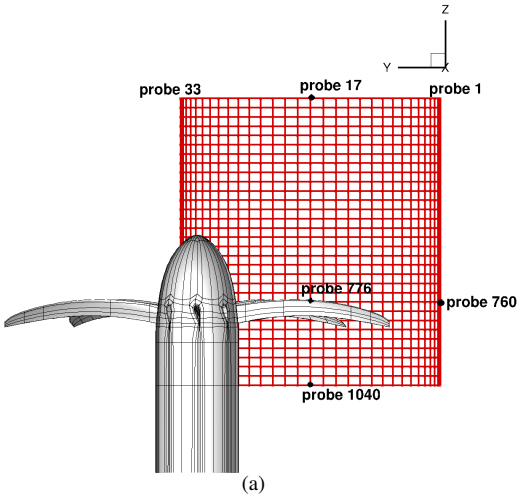

(a)

Figure 9: Probe positions for monitoring the propeller acoustics.

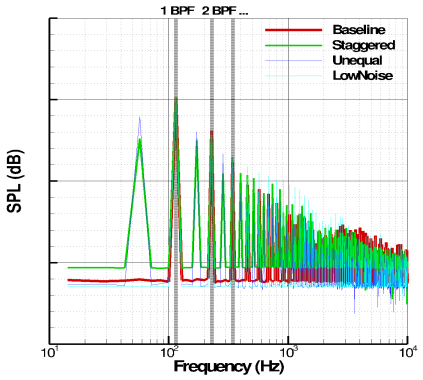

(a)

Figure 10: SPL vs. Frequency(Hz) for the various configurations with the baseline blade at probe 776. Cruise conditions, free-stream Mach = 0.5, tip Mach = 0.627, RANS calculations.

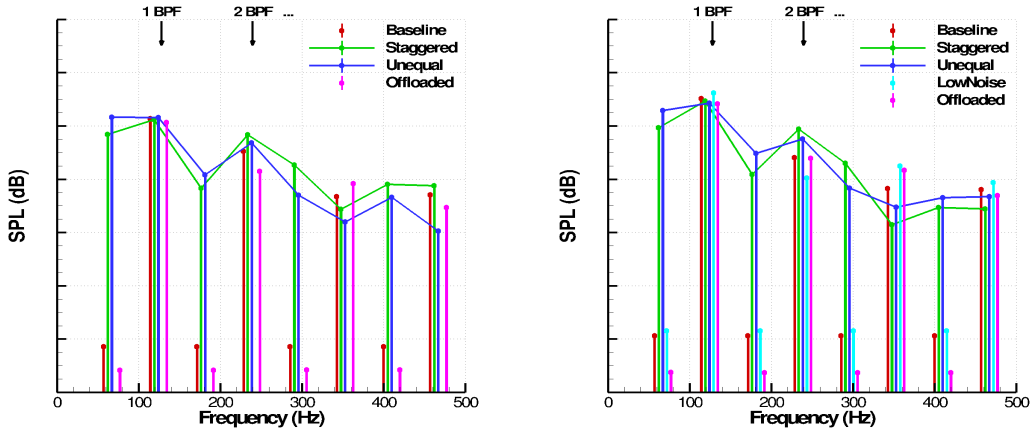

(a)

(b)

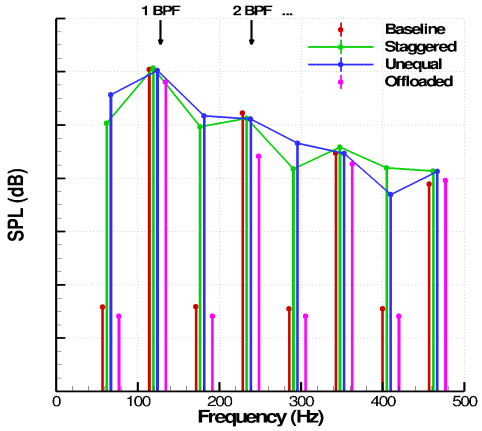

(c)

Figure 11: SPL at the Blade Passing Frequencies (BPF)(Hz) for the Baseline, Unequal and Staggered blades at three probe locations: (a) probe 760, (b) probe 792 and (c) probe 776. Cruise conditions, free-stream Mach = 0.5, tip Mach = 0.627, RANS calculations.

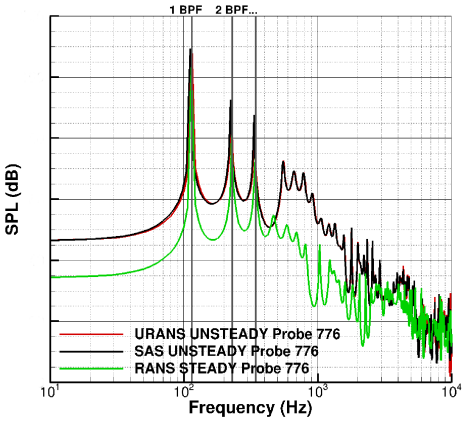

(a)

Figure 12: SPL vs. Frequency (Hz) for the Baseline at probe 776, cruise conditions, free-stream Mach = 0.5, tip Mach = 0.627 comparing SAS, URANS and RANS methods.

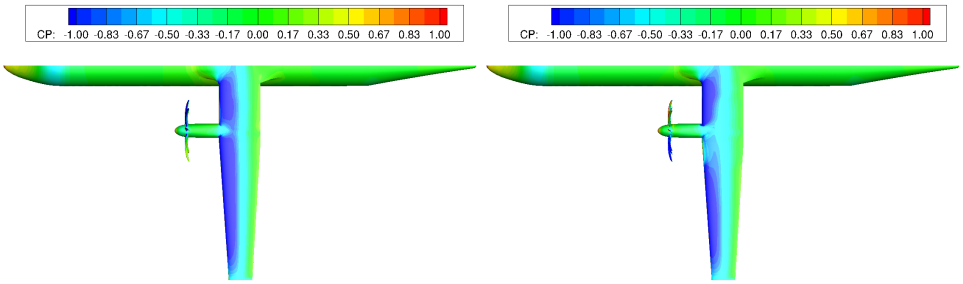

(a) (b)

Figure 13: Surface C_p for the installed baseline propeller. (a) Cruise conditions (b) Climb conditions as per Table 1.

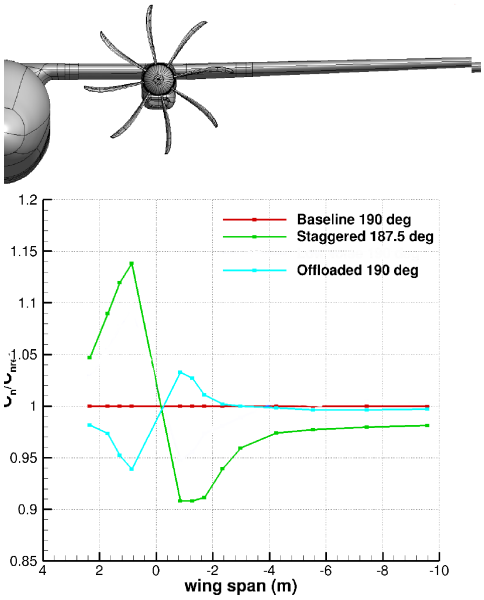

(a)

Figure 14: Wing loading with the different propellers when the blade vertically upwards is at 190 degrees azimuth at cruise conditions, free-stream Mach = 0.5, tip Mach = 0.627. 2nd revolution. The blade loading is given as a ratio of the blade loading on the baseline case.

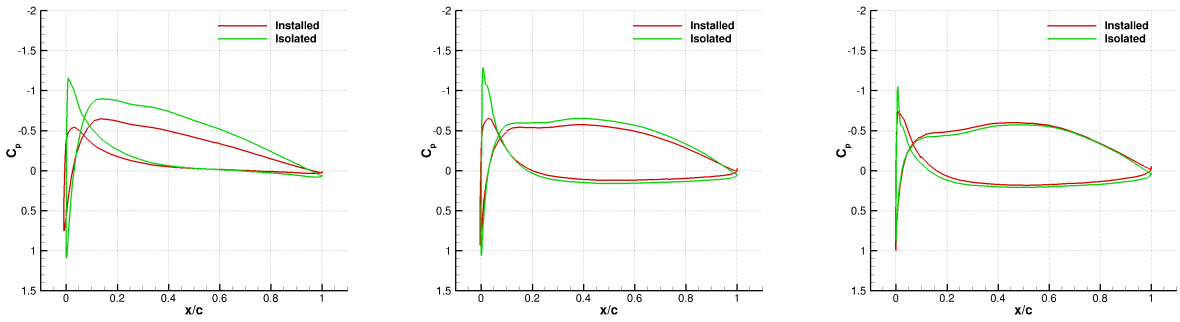

(a) r/R = 0.5 (b) r/R = 0.7 (c) r/R = 0.9

Figure 15: C_p on the blade at 0 degrees azimuth where blade is vertically upwards at cruise conditions in comparison with Isolated blade for the Baseline case.

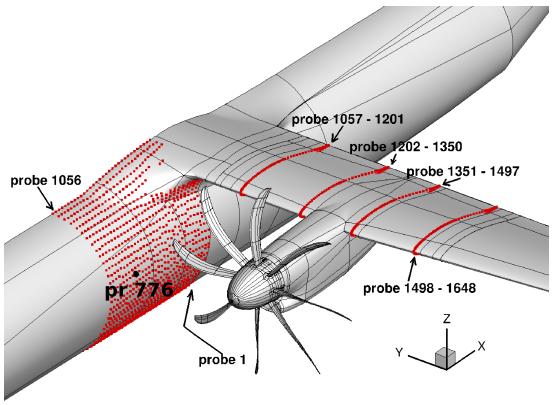

(a)

Figure 16: Probe locations for the installed cases.

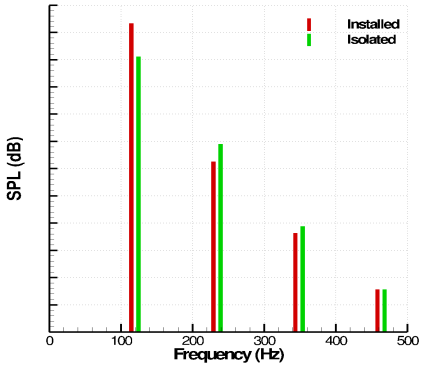

(a)

Figure 17: SPL vs. Frequency for probe 776 (middle of the fuselage in line with the propeller plane) with the isolated and installed cases. Cruise conditions, free-stream Mach = 0.5, tip Mach = 0.627.